Journal of Biomedical Optics

SPIEDigitalLibrary.org/jbo

Detachable microsphere scalpel tips for potential use in ophthalmic surgery with the erbium:YAG laser

Thomas C. Hutchens
Arash Darafsheh
Amir Fardad
Andrew N. Antoszyk
Howard S. Ying
Vasily N. Astratov
Nathaniel M. Fried

SPIE

Detachable microsphere scalpel tips for potential use in ophthalmic surgery with the erbium:YAG laser

Thomas C. Hutchens,[a,†] Arash Darafsheh,[a,†,‡] Amir Fardad,[b] Andrew N. Antoszyk,[c] Howard S. Ying,[d] Vasily N. Astratov,[a,*] and Nathaniel M. Fried[a,*]
[a]University of North Carolina at Charlotte, Department of Physics and Optical Science, Charlotte, North Carolina
[b]PhotonTech LLC, Durham, North Carolina
[c]Retina Service, Charlotte Eye Ear Nose and Throat Associates, Charlotte, North Carolina
[d]Johns Hopkins University, Wilmer Eye Institute, Baltimore, Maryland

Abstract. Vitreoretinal surgery is performed using mechanical dissection that sometimes results in iatrogenic complications, including vitreous hemorrhage, retinal breaks, incomplete membrane delamination, retinal distortion, microscopic damage, etc. An ultraprecise laser probe would be an ideal tool for cutting away pathologic membranes; however, the depth of surgery should be precisely controlled to protect the sensitive underlying retina. The ultraprecise surgical microprobe formed by chains of dielectric spheres for use with the erbium: YAG laser source ($\lambda = 2940$ nm), with extremely short optical penetration depth in tissue, was optimized. Numerical modeling demonstrated a potential advantage of five-sphere focusing chains of sapphire spheres with index $n = 1.71$ for ablating the tissue with self-limited depth around 10 to 20 μm. Novel detachable microsphere scalpel tips formed by chains of 300 μm sapphire (or ruby) spheres were tested on ophthalmic tissues, *ex vivo*. Detachable scalpel tips could allow for reusability of expensive mid-infrared trunk fibers between procedures, and offer more surgical customization by interchanging various scalpel tip configurations. An innovative method for aiming beam integration into the microsphere scalpel to improve the illumination of the surgical site was also shown. Single Er:YAG pulses of 0.2 mJ and 75-μs duration produced ablation craters in cornea epithelium for one, three, and five sphere structures with the latter generating the smallest crater depth (10 μm) with the least amount of thermal damage depth (30 μm). Detachable microsphere laser scalpel tips may allow surgeons better precision and safety compared to mechanical scalpels when operating on delicate or sensitive areas like the retina. [DOI: 10.1117/1.JBO.19.1.018003]

Keywords: erbium:YAG laser; light focusing; microspheres; ophthalmic surgery.

Paper 130734PR received Oct. 9, 2013; revised manuscript received Dec. 15, 2013; accepted for publication Dec. 18, 2013; published online Jan. 20, 2014.

1 Introduction

As of 2004, 4.1 million people in the United States suffered some form of diabetic retinopathy, and that number has steadily increased each year.[1] The current surgical procedure for proliferative diabetic retinopathy requires the tedious use of steel instruments to remove deposits off of the retina.[2] The tools access the vitreous cavity and pathologic fibrovascular tissue on the retinal surface through the pars plana. Removal of the fibrovascular membranes from the retina is the most important yet most tedious aspect of vitreoretinal surgery. Retinal membranes are segmented using a combination of automated vitreous cutters, membrane peeling and cutting scissors, and manual scissors. Delamination with forceps or scraping with picks or creating space between the membrane and retina for mechanical segmentation all stress the retina, increasing the risk for retinal tear or other damage.

A laser scalpel would be the logical advancement from these instruments. Over 20 years ago, the erbium:YAG laser was identified as a promising candidate for precise surgery[3–17] due to strong water absorption in soft tissues at its emission wavelength of $\lambda = 2.94$ μm. However, this laser did not gain widespread acceptance in vitreoretinal surgery due to its relatively large size, slow rate of tissue cutting, and necessity for bulky and exotic flexible mid-infrared (IR) delivery systems. In addition, the cutting rate was limited by vaporization bubbles that obstructed the view and made the judgment more difficult. This necessitated repeated exchange of instruments to remove the debris and regain control over the surgical field. Other lasers have also been extensively used in intraocular surgery; however, major drawbacks include difficulty in controlling the working distance, excessive depth of thermal damage, and difficulty in performing contact surgery.

Another hurdle to overcome is represented by the limited focusing capability of current microprobes used in surgery. The mid-IR flexible delivery systems such as fibers and hollow waveguides (HWGs) are usually multimodal, which makes beam focusing very difficult. Over the past two decades, various optical elements including spheres,[18] hemispheres, domes, cones, slanted shapes,[19,20] cylindrical gradient index lenses,[21] and tapered fibers have been tested as ophthalmic laser probe tips. It should be noted that these devices are usually designed to operate in noncontact mode in air and they lose their focusing capability in contact with tissue. In addition, in noncontact mode, the working distance is difficult to control during surgery and may result in large (>0.1 mm) and variable beam sizes in tissue. It is interesting to note that using high index spheres, the

†These authors contributed equally to this work.
‡Present address: Department of Radiation Oncology, University of Pennsylvania, Philadelphia, PA

*Address all correspondence to: Vasily N. Astratov, Email: Astratov@uncc.edu; Nathaniel M. Fried, E-mail: nmfried@uncc.edu

focusing can be provided just at the tip of the device thus making the position of the maximal irradiance less sensitive to the presence of the external medium.[22,23]

Using similar ideas, recently, we proposed to develop a surgical system with an extremely compact focal spot and shallow depth of treatment, which can be used for segmenting pathologic epiretinal membranes without damaging the adjacent retina.[22–27] To this end, we developed the design of fiber-based microprobes capable of focusing light under contact conditions with tissue.[25] Specifically, we showed that a chain of microspheres with index $n = 1.71$ is capable of focusing the beam at the tip of the end sphere with essentially zero focusing depth. In addition, the device is capable of compact focusing of multimodal beams delivered by fibers or HWGs used in mid-IR optics. We showed that this occurs due to the filtering of novel type of optical modes with the radial state of polarization termed periodically focused[28] or nanojet-induced modes.[29,30]

Compared to mechanical tools and alternative laser devices, our device has numerous potential advantages including: (i) improved surgical precision and control due to small lateral spot diameter (~20 to 30 μm) when in contact with strongly absorbing tissue, (ii) reduction in intraocular bleeding due to ablating tissue through photothermal laser-tissue interaction, (iii) reduction in trauma from blunt dissection, and (iv) high cutting rates due to a possibility of using newer electronically modulated diode-pumped lasers with $\lambda \sim 3$ μm operating at much higher pulse rates (up to 2000 Hz).

We tested the optical scalpel using *ex vivo* porcine corneas as a simple, robust ophthalmic tissue model.[26,27] The ablation threshold for *ex vivo* porcine cornea samples was found to be ~1.3 J/cm^2 (pulse energy ~25 μJ, FWHM spot diameter ~50 μm). This ablation threshold corresponds well with that reported in previously published studies, 0.1 to 1.0 J/cm^2 using the Er:YAG laser for ablation of various soft tissues.

Although these results showed the potential advantages of using such a device in intraocular laser surgery, the design of the focusing structure was suboptimal in our previous studies.[26,27] The focusing was provided slightly in front of the end sphere which, in principal, should lead to deeper ablation craters that is not consistent with the goals of this surgery aimed at dissecting and laminating of the fibrotic membranes with controllable and shallow depth. The suboptimal feature of this previous design was due to the fact that all scalpels tested contained a larger diameter glued distal sphere (350 μm) followed by smaller diameter (300 μm) spheres inside the HWG to generate the odd-numbered focusing chains. The reason for selecting this structure was connected with difficulties in the fabrication of optimal structures formed by uniform size spheres.

In this work, we solved the problem of assembly of optimal structure formed by chains of identical sapphire spheres with $n = 1.71$. This problem was solved by tightly packing microspheres inside plastic tubing and integrating this tube within the waveguide. By using numerical modeling, we show that the optimal structures focus light exactly at the tip of the end sphere which leads to an important advantage of these structures for achieving shallow and well controllable depth of surgery. The cavitation bubble inevitably occurs in such surgeries near the tip of the device. We show, however, that in the optimally designed structures the beam is extremely divergent inside such bubbles which should significantly slow down the depth of tissue ablation once the size of the bubbles reaches ~10 μm. This mechanism can be considered as a built-in safety feature for reducing the retina damage in the course of dissecting unhealthy fibrotic membranes or other ultraprecise surgical procedures. Finally, we demonstrate possible packaging techniques that allow for detachable tips with integrated illumination.

2 Theoretical Modeling

Theoretical modeling was performed with Zemax (Radiant Zemax LLC, Redmond, Washington, USA), a commercial optical design software package. The main components were the laser light source, laser delivery system, and focusing elements. As illustrated in Fig. 1, it was assumed that a multimode fiber (e.g., germanium oxide fiber) with a core diameter of $2a = 150$ μm and with NA = 0.12 was inserted into an HWG (a hollow glass waveguide) with an internal diameter of $2a = 300$ μm. These dimensions are typical for mid-IR waveguides.[31] Smaller HWG diameters would allow more compact focusing of the beams; however, diameters smaller than $2a = 300$ μm are rarely used in practice because of the strongly increasing propagation losses $\alpha \sim 1/a^3$, where α is the attenuation coefficient.[31] The first sphere was placed close to the HWG edge in a configuration where half of the end sphere was extended from the HWG as depicted in Fig. 1 for a five sphere chain. An absorbing tubing was placed around the sphere chain to simulate Tygon tubing used in construction. In our previous studies, such a structure was optimized for the best performance in contact with tissue.[25] We showed that the minimal spot sizes and combination with good coupling efficiency can be obtained in chains of 300 μm spheres with the index around $n = 1.71$. The calculated irradiance profiles after three and five spheres

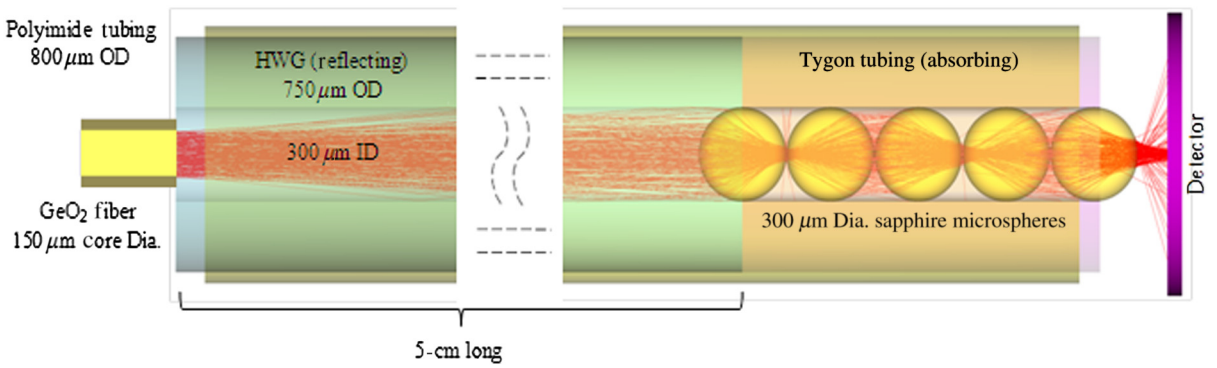

Fig. 1 A focusing mid-infrared (IR) microprobe design based on chains of spheres placed in a hollow waveguide (HWG).

show twofold spot size reduction compared to single sphere. The FWHM of ~6 μm is calculated for chains of five spheres.

To model the device operation in the presence of cavitation bubbles, we placed the detector at different distances from the tip of the device in the medium with $n = 1$ [Fig. 2(a)] and calculated the beam profile at different distances from the tip, as illustrated in Figs. 2(b)–2(d) for $N = 1$, 3, and 5 sphere chains, respectively. In a real surgical environment, the vaporized tissue would create a bubble just at the tip of the sphere, and the light would propagate through this bubble. In our modeling, we neglected the light absorption inside the bubble and assumed that the vapor index was close to $n = 1$. The irradiance profiles in Figs. 2(b)–2(d) effectively represent the irradiance distribution at the bubble sidewall at various depths. The green dashed lines are used as a guide to represent how the irradiance peak of the beam reaching the opposite sidewall of the bubble depends on the bubble diameter. It is seen that for a single sphere and three sphere chain the irradiance peak experiences slow variations as the bubble grows. The irradiance peak for the five sphere chain shows a peculiar behavior which can be very useful for controlling the depth of surgery. Once the bubble reaches about 10 μm size, the irradiance peak drops by a factor of four and stays at this low level for bubble sizes increasing up to 20 to 30 μm. This situation indicates a possibility that the depth of the ablation craters in tissue would saturate at the 10 to 20 μm level in practical surgery.

The mechanism of light focusing by such structures is based on the properties of so-called periodically focused modes (PFMs)[28] schematically illustrated in Fig. 2(a) using red color. These modes have cylindrical symmetry in radial direction and period equal to the size of two spheres along the axis of the chain. Unusually high transmission properties of PFMs can be understood due to the fact that corresponding rays intersect the spherical interfaces under Brewster angle condition for transverse magnetic polarization and, as a result, they are not reflected. It can be shown that these modes play a dominant role in the optical transmission properties of such chains for $n \sim 1.70 - 1.75$.[28] Although the rays with different off-axial offsets and angles of incidence are coupled into such chains from the source, only PFMs survive in sufficiently long chains. The fact that PFMs have two-dimensional (2-D) period for spheres with a moderate index of refraction ($n < 2$) can be understood due to significant spherical aberrations introduced by large lateral offset of these modes. This is especially clear in comparison with the case of propagation of paraxial and close to paraxial rays also shown in Fig. 2(a) using blue color. It is seen that

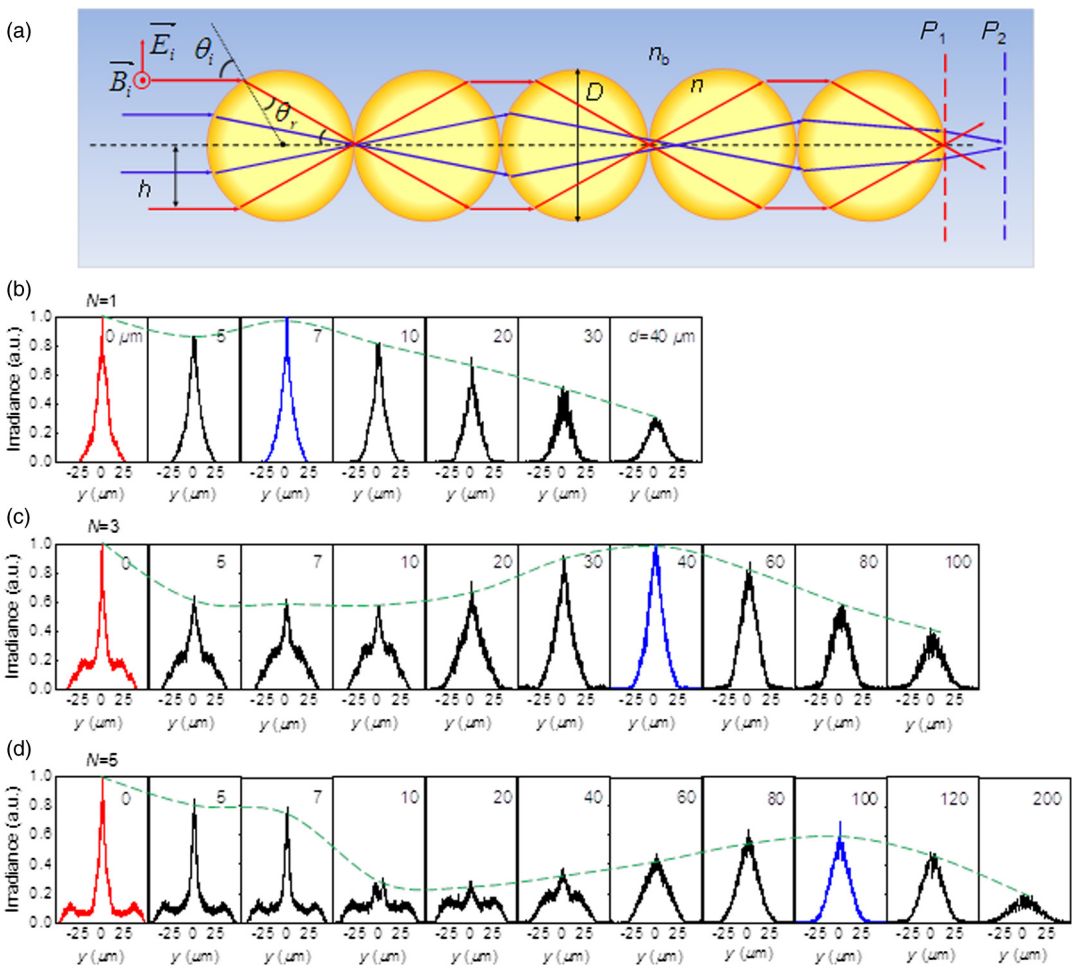

Fig. 2 (a) Different depth of focuses for different modes based on spherical aberrations in odd-numbered sphere chains. Red rays correspond to periodically focused modes (PFMs) which focus at the surface of every odd number of spheres. Blue rays correspond to paraxial rays. (b–d) Irradiance distributions are shown for different distances from the tip of a microprobe composed of one, three, and five spheres with $n = 1.71$.

these rays have a period longer than 2-D which is expected for $n = 1.71$ due to the absence of spherical aberrations for paraxial rays. As a result, the paraxial modes cannot be used for focusing light at the tip of the end sphere. In addition, they tend to be attenuated much stronger in such structures in comparison with PFMs due to the fact that they intersect spheres at variable angles which are, generally, different from the Brewster angle. Figures 2(b)–2(d) show the approximate location of the paraxial focus depth in blue, which is forced deeper in longer chains, beyond the effect of the mid-IR energy which has an ~10 μm optical penetration depth.

The sharp focusing of light at the tip of the end sphere for the five sphere chain illustrated in Fig. 2(d) is explained by the PFM filtering effects.[28] These chains are sufficiently long to suppress paraxial and other modes except PFMs. So, due to the precise 2-D periodicity, the PFMs can be focused at the tip of the end sphere with an extremely small focusing depth of ~7 to 10 μm. The reduction of the irradiance at longer distances can be simply explained by the strongly divergent nature of PFMs. This property of the PFM can act as a factor limiting the depth of surgery. When the probe is in contact with tissue, it provides sharp focusing and locally ablates the tissue creating a vapor bubble. Once a gap between the tip and underlying tissue is created, the irradiance peak drops due to the PFM short focusing depth which reduces the tissue ablation rate.

The vapor or cavitation bubble effect of the erbium:YAG laser operating in normal spiking mode has been previously studied at larger pulse energies and smaller energy densities.[21] In this study, the full width pulse duration was measured to be 75 μs; however, the highest peak power occurred within the first few microseconds of the initial spike.[26] With the microsphere scalpel having an extremely high output numerical aperture and using a low pulse energy, we believe these cavitation effects are spatially small, isotropic, and on the order of a few microseconds. During the bubble, the mid-IR light attenuation drops allowing for deeper propagation, however, as seen in Fig. 2(d) for the five sphere configurations, the beam intensity also drops significantly at 10 μm from the sphere tip counteracting this effect. This is what is referred to as "self-limiting ablation depth" in this work.

It should be noted that achieving well-controlled self-limiting ablation depth also requires some adjustments for the pulse energy which should be higher than the ablation threshold, but not excessively high. This can be understood based on considering the time scale for the bubble formation. The optimal regime for self-limiting ablation implies that the bubble formation would slow down at the end of each pulse. On the other hand, if the excessively high pulse energy is used, the "slowing" effect would take place only in the beginning of each pulse when the bubbles reach optimal 10 to 20 μm dimensions. The continuing exposure within each pulse would cause the bubble to grow beyond these limits. In the latter case, as seen in Fig. 2, the level of irradiance at the back surface of the bubble should increase again so that would make invalid the mechanism of "self-limiting ablation depth".

3 Materials and Methods

3.1 *Microsphere Scalpel Detachable Tip with Illumination*

To create the microsphere scalpel with identical sphere diameters, a flexible Tygon tube (ColeParmer Instrument Company, Vernon Hills, Illinois, USA) with an inner diameter (ID) of 250 μm was used to secure the 300-μm diameter sapphire (or ruby) spheres (Swiss Jewel Company, Philadelphia, Pennsylvania, USA), as shown in Fig. 3. The tight-fitting Tygon tubing provided a waterproof seal at the distal tip. The sphere chain was then placed in front of the HWG with the inner and outer diameters of 300 and 750 μm, respectively, and both were secured together inside a thin-wall polyimide tube (B000PHAI3M, Amazon Supply, Seattle, Washington, USA). A small ring of glue was then applied to secure the polyimide to the Tygon tubing.

Previous studies were performed with a probe created by inserting and fixing a flexible, 2-m long, 200-μm-outer diameter (OD) germanium oxide fiber into the proximal end of the HWG.[26,27] In this work, a simple self-aligning detachable tip was created by gluing the proximal end of the HWG inside a 770-μm-inner diameter SMA connector (10770A, Thorlabs, Newton, New Jersey). A custom dual fiber connector (Fig. 4) and the HWG connector were then joined with an SMA mating sleeve (ADASMA, Thorlabs). Using an HWG with a length of 5 cm allowed for a probe needle length of about 3 cm, or roughly the length of current intraocular instruments (Fig. 5).

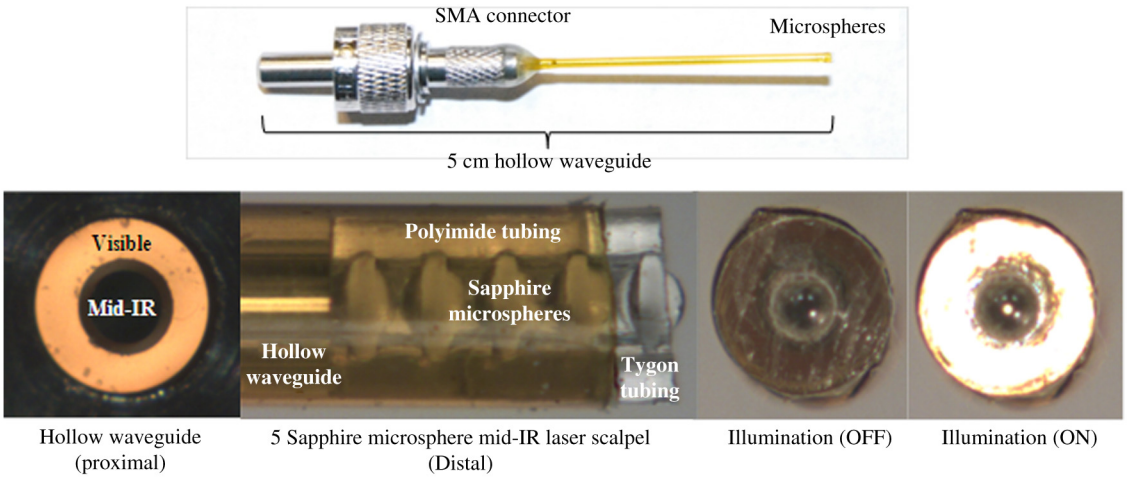

Fig. 3 Detachable microsphere scalpel tip with integrated illumination. A standard sub multi assembly (SMA) fiber connector was secured to the proximal end of the HWG.

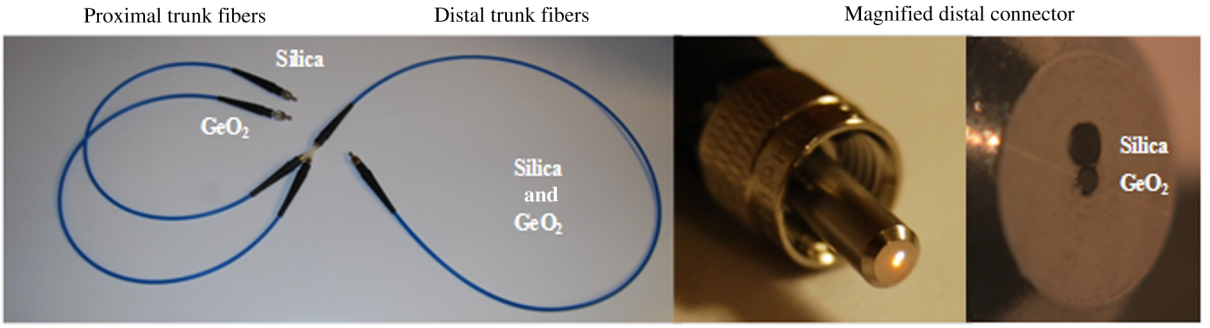

Fig. 4 Custom dual fiber optic cable. Singular 150-μm core diameter germanium oxide (mid-IR) and 300-μm core diameter silica (visible) fibers are combined at a Y-junction into a two fiber bundle with the germanium oxide (GeO_2) fiber central on the distal connector.

3.2 *Laser Source and Custom Fiber Delivery*

An erbium:YAG laser (Model 1-2-3, Schwartz Electro-Optics, Orlando, Florida, USA) operating at a wavelength of 2940 nm, in normal-spiking mode with a pulse duration of 75 μs, and a pulse rate of 5 Hz was used in these experimental studies. A 2-m long, 150-μm core diameter, 200-μm-OD germanium oxide mid-IR optical fiber (Infrared Fiber Systems, Silver Spring, Maryland, USA) was used to guide the laser energy into the core of the silica HWG (HWEA300750, Polymicro Technologies, Phoenix, Arizona, USA) used in the scalpel. The fiber core has a refractive index of 1.84 with an attenuation of 0.7 dB/m at a wavelength of 2940 nm.

Typical visible aiming beam or illumination coupling into the germanium oxide fiber is possible; however, the extremely tight focusing at the end sphere would provide minimum illumination for the surgeon. Improved illumination functionality was achieved using the fact that the cladding of the mid-IR HWG made from silica can be used as a waveguide for visible light, generating more widespread light to the surgical region. A separate 300-μm core diameter silica fiber (FIP300330370, Polymicro Technologies) coupled to a white light source was used to deliver illumination light to the silica cladding region of the HWG in the scalpel. This was achieved by drilling an offset 350-μm diameter hole adjacent to the standard central 230-μm hole in an SMA fiber optic connector (10230A, Thorlabs). The germanium oxide and silica fibers were placed in the central and offset holes, respectively (Fig. 4). At some distance along the trunk, the two fibers were split into separate trunks at a Y-junction and connectorized with standard single hole SMA connectors, as shown in Fig. 4 (left). All fiber sections were then encased in a Kevlar protective fiber jacket (FT030, Thorlabs). When mated in a sleeve (ADASMA, Thorlabs), this allowed the germanium oxide and silica fibers (Fig. 4) to self-align with the HWG's inner hollow channel and outer silica region (Fig. 3), respectively, resulting in a typically sized scalpel with detachable and disposable tips (Fig. 5).

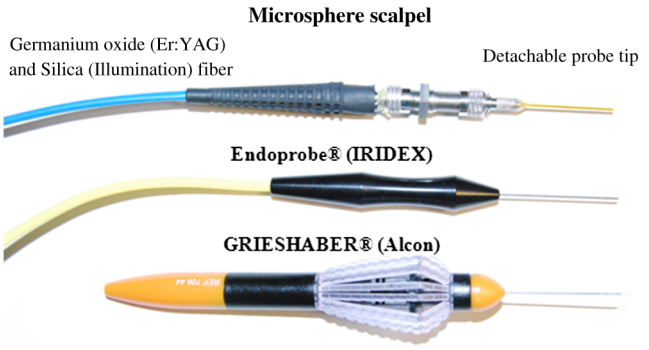

Fig. 5 Detachable microsphere scalpel prototype (~800-μm OD) compared to two common ocular surgical instruments, each of which are 23 gauge (~625 μm). For the microsphere scalpel, two standard SMA fiber connectors are integrated using a mating sleeve.

3.3 *Experimental Tissue Setup*

Fresh porcine eyes were harvested and used immediately after sacrifice of pigs at a local slaughterhouse. The cornea was chosen in this preliminary study as a simple model for ophthalmic tissue ablation experiments for several reasons, including its ease of use concerning dissection, preservation, processing, and analysis after laser tissue ablation. Preliminary test results performed on retinal tissue were not shown because our current capabilities hinder us from recording measurements on retinal craters. This was due to the fact that the microscopic ablation craters were difficult to distinguish visibly, and our histological fixation methods induced a large amount of stress on the fragile retina therefore destroying the samples.

Tissue ablation experiments were then performed by bringing the cornea tissue into gentle contact with the various probe configurations and translating the sample, *ex vivo*. The cornea was kept hydrated prior to each test by applying a single drop of tetrahydrozoline HCl 0.05%, common over the counter eye drop solution. The relatively low laser pulse rate of 5 Hz allowed creation of hundreds of single pulse craters along this path over a period of 60 s.

4 Results

Single pulse craters were formed on hydrated cornea tissue using a pulse energy of ~0.2 mJ. The pulse energy was measured using a pyroelectric detector (ED-100A, Gentec, Saint-Foy, Canada) near the tip of the probe. Single, three, and five sphere structures of identical sphere size were tested and since each sphere chain configuration (one, three, or five spheres) attenuated the energy differently, attenuation of the laser output was adjusted to normalize each configuration to an incident energy of ~0.2 mJ on the tissue surface. The fixed pulse energy of 0.2 mJ corresponds to a pulse energy within an order of magnitude above the ablation threshold (~1 J/cm^2) for the one sphere configuration, but held constant for other configurations for better comparison. The transmission losses in such chains are significantly reduced as light propagates along the chain. The adjustments to the laser attenuation

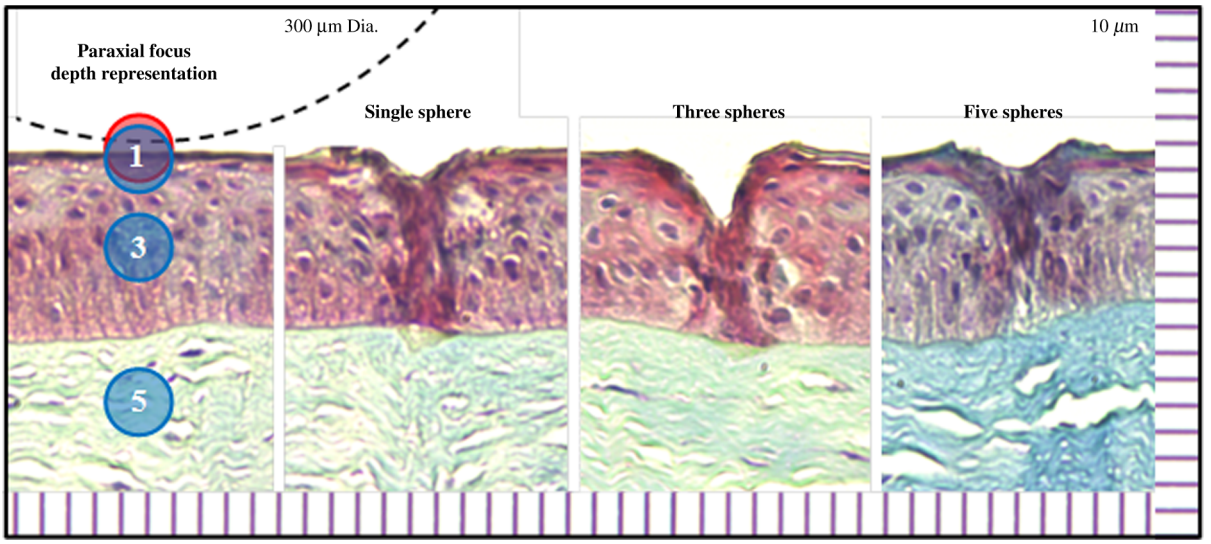

Fig. 6 Trichrome histology of ablation craters created in the epithelium layer of porcine cornea using a detachable microsphere scalpel with integrated illumination. The dashed line illustrates the physical scalpel tip with 300-μm diameter for size comparison. The red and blue dots represent the theoretical focal depth for periodic-focused modes and paraxial modes in native tissue, respectively, modeled in Fig. 2.

for each configuration were performed to compensate for the increased transmission loss in longer sphere chains. The major contributor to transmission loss (Fresnel reflection) was approximated to be an additional 25% between each configuration, corresponding to four sapphire/air ($n = 1.71/1$) surfaces. It should be noted, however, that as light propagates through the chain, the losses become progressively smaller reaching extraordinarily small values ~0.1 dB/sphere far away from the illumination source. This is explained by gradual filtering of PFMs in such chains. These modes intersect spherical interfaces under Brewster angle conditions that greatly minimize the losses. Transmission through sphere chains was explained in the previous work.[25]

Due to tissue transparency, histologic analysis was performed on the corneas to quantify ablation crater and thermal damage depths. Immediately after the procedure, the eyes were placed in formalin. With the pupil center being the pole, the eyes were sectioned latitudinal and the extra material was discarded leaving only the polar cornea region. The corneas were trimmed to ~1-mm thick longitudinal for histological processing and various samples were stained with Masson's Trichrome. The craters were viewed and measured using a microscope equipped with a CCD camera. A representative image for each sphere configuration is shown in Fig. 6. An additional native cornea histology image is shown to visualize the PFM and paraxial foci of the 300-μm diameter sphere configurations. Ablation craters depths of 12, 25, and 10 μm and thermal damage depths of 70, 40, and 30 μm were measured for one, three, and five spheres, respectively. Although tissue staining was inconsistent between batches, the darker colored region in each image represents thermal damage. The tearing and folding observed in the histology images, particularly in the stroma region (blue stained) for the one and five sphere configurations was an artifact of the histological processing, extending laterally far beyond the treatment area into the native tissue, and was therefore not indicative of tissue damage caused by the laser. However, some slight alteration in the stroma can be seen for the one and three sphere configurations (yellow stained), corresponding to deeper thermal damage in those cases.

5 Discussion

Short ablation depths with small thermal damage regions have been achieved with Er:YAG laser probes in the previous studies.[3–17,32] However, our contact mode mid-IR microsphere scalpel can create spatially small ablation craters below the limit of current intraocular fiber delivery systems, while using a less powerful laser source. Sapphire microspheres with a refractive index of 1.71, used as lenses, focus laser light at the sphere's surface creating a robust contact laser device where the transmission medium will not affect the device's performance. By building these sphere chains inside an air filled HWG's tip and sealing it to the end sphere, all internal focusing surfaces maintain their relative refractive indices even when submerged in the vitreous.

Ablation crater depths on corneal tissue were measured between 10 and 25 μm. Previous studies[26,27] were performed with a less optimal larger end sphere and at a pulse energy of ~0.1 mJ. In contrast, this study used identical diameter spheres and a pulse energy of ~0.2 mJ. The much smaller depth of ablation craters and more compact thermal damage zone observed for the five sphere chain is due to the mechanism of self-limiting depth of surgery discussed in Sec. 2 and schematically illustrated in Fig. 2. Although retinal tissue has different optical and mechanical properties than cornea, by using the Er:YAG laser which has such a strong water absorption peak, future retinal tissue ablation results may be comparable. Removal of small deposits with thicknesses between 20 and 50 μm on top of the retina, while minimizing damage to the retina which has a thickness ranging between 150 and 300 μm, is the primary goal of this scalpel design.

The purpose of the left section of Fig. 6 is to better illustrate the scale of the sphere to the corneal layer tested as well as overlay the approximate focal points of the paraxial rays shown in Fig. 2. The one sphere case shows that the PFM and paraxial focus are near the sphere's surface which combine to form a spatially larger, and not self-limiting ablation depth causing deeper thermal damage beyond the crater and reaching the stroma. However, the crater is shallow corresponding to a

drop-off in energy density as seen in Fig. 2. For the three sphere case, the energy density does not drop off significantly immediately because the PFM combined with the paraxial modes form a thinner but longer region for ablation up to a ~40-μm depth, which is achievable with the erbium:YAG laser due to cavitation bubble effects. However, for the five sphere case, the paraxial modes are focused too deep into the tissue to have any significant effect on energy density at the surface, and since the five sphere chain's intensity drops off significantly at ~10-μm depth, the crater and thermal damage are shallower.

Although not observed or characterized in this preliminary study with corneal tissues, it is possible that exploding and imploding vapor bubbles at the treatment site may result in mechanical damage to other more delicate ophthalmic tissues of interest such as the retina, which do not have the same robust mechanical properties as the cornea. We believe that these bubbles are highly localized and shallow, and therefore will not cause significant mechanical tissue damage due to the low pulse energy, small spot diameter, and contact mode application of our probe. In our theoretical model, we assumed that these cavitation bubbles, which are formed almost immediately at the beginning of each pulse, act as a low absorption conduit to allow the Er:YAG laser energy to travel deeper into the tissue. The Er:YAG laser only has an optical penetration depth of ~10 μm in water at high temperatures; however, the longer pulse duration could be responsible for the depths of thermal heating measured in the histology. Due to the bubbles' small size and rapid dispersion they should not obscure the surgeon's vision. However, further detailed studies utilizing a high-speed camera to directly image the cavitation bubble dynamics during mid-IR ablation of both corneal and retinal tissues will be necessary in future work to confirm these claims.

Regarding the use of such ultraprecise laser scalpels in the intraocular surgery, it should be noted that it might be suitable for cutting and delaminating of the membranes rather than for their areal ablation. The speed of cutting can be significantly increased by using diode-pumped erbium:YAG lasers with the higher pulse repetition rates on the order of 1000 Hz. Use of the proposed device in combination with the mechanical tissue holders and picks may be helpful for reducing the surgical time and achieving the best surgical outcomes. More studies are required to develop the actual surgical procedures; however, it is apparent that the safety and high speed of tissue cutting may be potential advantages for such ultraprecise laser scalpels.

By integrating multiple functions like illumination into a single ophthalmic handpiece, the singular surgeon also gains more surgical freedom for simultaneous use of other devices in the otherwise occupied hand. We have improved upon the previous single function microsphere probe by integrating enhanced illumination into the otherwise wasted space of the HWG. Also by making the microsphere scalpel detachable and disposable between procedures, the expensive germanium oxide trunk fiber is preserved representing significant cost savings. Other instruments commonly used in intraocular surgery could also be integrated with the microsphere scalpel. The most obvious is the vitrector or the suction device used to remove debris from the vitreous. By placing a vitrector tip directly adjacent to the microsphere scalpel, any debris created from the ablated tissue or small sections of tissue cut free by the scalpel is instantly removed from the surgical site. However, the current microsphere scalpel is considered a 20 gauge (~900-μm OD) instrument, which is on the large side of current instruments which are 25+ gauge (~500-μm OD).[33,34] It may be possible to replace the large HWG and miniaturize the microsphere scalpel, since the key optical components are the 200-μm-OD germanium oxide fiber and a chain of five 250 μm microspheres; however, preliminary studies have shown larger contact-mode spatial beam diameters when putting the fiber in direct contact with the microsphere chain.

6 Conclusions

Ophthalmic surgery may benefit from the use of more precise fiber optic delivery systems during laser surgery. In this study, an optimized detachable tip laser scalpel consisting of chains of sapphire (or ruby) microspheres positioned at the distal tip of an HWG was successfully tested on *ex vivo* cornea tissue. One, three, and five microsphere chain structures were modeled, demonstrating a self-limiting short focal depth, especially for the five sphere chain. Single Er:YAG laser pulses of 0.2 mJ and 75-μs duration produced ablation craters in cornea epithelium for one, three, and five sphere structures with the latter generating the smallest craters with the least amount of thermal damage depth. Microsphere chains produced spatial filtering of the multimode Er:YAG laser beam and fiber, thus providing spot diameters not otherwise available using conventional fiber delivery systems. Integration of illumination with the microsphere scalpel could improve surgeon familiarity, performance, and eventual adoption. With further development, this novel approach to mid-IR laser ablation may provide an alternative to mechanical tools for surgical dissection and removal of ophthalmic tissues.

Acknowledgments

This work was supported by the U.S. Army Research Office through John T. Prater under Contract No. W911NF-09-1-0450 and by the National Science Foundation under Grant ECCS-0824067. The authors also gratefully acknowledge support for the initial work from the National Eye Institute under Award No. R41EY019598. The content is solely the responsibility of the authors and does not necessarily represent the official views of the National Eye Institute or the National Institutes of Health.

References

1. The Eye Diseases Prevalence Research Group, "The prevalence of diabetic retinopathy among adults in the United States," *Arch. Ophthalmol.* **122**(4), 552–563 (2004).
2. G. L. Spaeth, *Ophthalmic Surgery: Principles and Practice*, Saunders, Philadelphia (1982).
3. S. A. Ozler et al., "Infrared laser sclerostomies," *Invest. Ophthalmol. Vis. Sci.* **32**(9), 2498–2503 (1991).
4. R. A. Hill et al., "Laser trabecular ablation (LTA)," *Lasers Surg. Med.* **11**(4), 341–346 (1991).
5. M. L. McHam et al., "Erbium:Yag laser trabecular ablation with a sapphire optical fiber," *Exp. Eye Res.* **65**(2), 151–155 (1997).
6. G. Stevens, Jr. et al., "Erbium:YAG laser-assisted cataract surgery," *Ophthal. Surg. Lasers* **29**(3), 185–189 (1998).
7. P. D. Brazitikos et al., "Experimental ocular surgery with a high-repetition-rate erbium:YAG laser," *Invest. Ophthalmol. Vis. Sci.* **39**(9), 1667–1675 (1998).
8. C. C. Neubaur and G. Stevens Jr., "Erbium:YAG laser cataract removal: role of fiber-optic delivery system," *J. Cataract. Refract. Surg.* **25**(4), 514–520 (1999).
9. T. Wesendahl et al., "Erbium:YAG laser ablation of retinal tissue under perfluorodecaline: determination of laser-tissue interaction in pig eyes," *Invest. Ophthalmol. Vis. Sci.* **41**(2), 505–512 (2000).

10. U. Hohenleutner et al., "Fast and effective skin ablation with and Er: YAG laser: determination of ablation rates and thermal damage zones," *Lasers Surg. Med.* **20**(3), 242–247 (1997).
11. J. T. Walsh, T. J. Flotte, and T. F. Deutsch, "Er:YAG laser ablation of tissue: effect of pulse duration and tissue type on thermal damage," *Lasers Surg. Med.* **9**(4), 314–326 (1989).
12. D. J. D'Amico et al., "Initial clinical experience with an erbium:YAG laser for viteoretinal surgery," *Am. J. Opthalmol.* **121**(4), 414–425 (1996).
13. D. J. D'Amico et al., "Multicenter clinical experience using an erbium: YAG laser for vitreoretinal surgery," *Ophthalmology* **103**(10), 1575–1585 (1996).
14. D. P. Joseph et al., "A new and improved vitreoretinal erbium:YAG laser scalpel: long term morphologic characteristics of retinal-choriodal injury," *Ophthal. Surg. Lasers Imaging* **35**(4), 304–315 (2004).
15. M. H. Krause and D. J. D'Amico, "Ablation of vitreous tissue with a high repetition rate erbium:YAG laser," *Eur. J. Ophthalmol.* **13**(5), 424–432 (2003).
16. H. Hoerauf et al., "Retinal photoablation with the erbium:YAG laser. Initial experimental results for traction-free removal of tissue," *Ophthalmologe* **100**(2), 115–121 (2003).
17. H. Hoerauf et al., "Photoablation of inner limiting membrane and inner retinal layers using the erbium:YAG laser: an in vitro study," *Lasers Surg. Med.* **38**(1), 52–61 (2006).
18. R. M. Verdaasdonk and C. Borst, "Ray tracing of optically modified fiber tips. 1: spherical probes," *Appl. Opt.* **30**(16), 2159–2171 (1991).
19. K. Iwai et al., "Penetration of high-intensity Er:YAG laser light emitted by IR hollow optical fibers with sealing caps in water," *Appl. Opt.* **43**(12), 2568–2571 (2004).
20. T. Watanabe and Y. Matsuura, "Side-firing sealing caps for hollow optical fibers," *Lasers Surg. Med.* **38**(8), 792–797 (2006).
21. D. X. Hammer et al., "Intraocular laser surgical probe for membrane disruption by laser-induced breakdown," *Appl. Opt.* **36**(7), 1684–1693 (1997).
22. V. N. Astratov et al., "Photonic nanojets for laser surgery," *SPIE Newsroom* (2010).
23. A. Darafsheh et al., "Integrated microsphere arrays: light focusing and propagation effects," *Proc. SPIE* **7605**, 76050R (2010).
24. A. Darafsheh et al., "Focusing capability of integrated chains of microspheres in the limit of geometrical optics," *Proc. SPIE* **7913**, 79131A (2011).
25. A. Darafsheh et al., "Contact focusing multimodal microprobes for ultraprecise laser tissue surgery," *Opt. Express* **19**(4), 3440–3448 (2011).
26. T. C. Hutchens et al., "Microsphere chain fiber tips for multimode filtering of erbium:YAG laser beam during contact tissue ablation." *Proc. SPIE* **8218**, 821803 (2012).
27. T. C. Hutchens et al., "Characterization of novel microsphere chain fiber optic tips for potential use in ophthalmic laser surgery," *J. Biomed. Opt.* **17**(6), 068004 (2012).
28. A. Darafsheh and V. N. Astratov, "Periodically focused modes in chains of dielectric spheres," *Appl. Phys. Lett.* **100**(6), 061123 (2012).
29. A. M. Kapitonov and V. N. Astratov, "Observation of nanojet-induced modes with small propagation losses in chains of coupled spherical cavities," *Opt. Lett.* **32**(4), 409–411 (2007).
30. S. Yang and V. N. Astratov, "Photonic nanojet-induced modes in chains of size-disordered microspheres with an attenuation of only 0.08 dB per sphere," *Appl. Phys. Lett.* **92**(26), 261111 (2008).
31. J. A. Harrington, "A review of IR transmitting, hollow waveguides," *Fiber Int. Opt.* **19**(3), 211–227 (2000).
32. J. W. Berger and D. J. D'Amico, "Modeling of erbium: YAG laser-mediated explosive photovaporization: implications for vitreoretinal surgery," *Ophthal. Surg. Lasers* **28**(2), 133–139 (1997).
33. A. Darafsheh et al., "Contact focusing multimodal probes for potential use in ophthalmic surgery with the erbium:YAG laser," *Proc. SPIE* **8567**, 856729 (2013).
34. F. M. Recchia et al., "Small-gauge pars plana vitrectomy: a report by the American Academy of Ophthalmology," *Ophthalmology* **117**(9), 1851–1857 (2010).

Biographies of the authors are not available.